Molecular Dissection of the Interaction between Amyloid Precursor Protein and Its Neuronal Trafficking Receptor SorLA/LR11[†]

Olav M. Andersen,*[,‡] Vanessa Schmidt,[‡] Robert Spoelgen,[§] Jørgen Gliemann,[||] Joachim Behlke,[‡] Denise Galatis,[⊥,#] William J. McKinstry,[△] Michael W. Parker,[△] Colin L. Masters,[⊥,#] Bradley T. Hyman,[§] Roberto Cappai,[⊥,#,◇] and Thomas E. Willnow[‡]

Max-Delbrueck-Center for Molecular Medicine, Berlin, 13125 Berlin, Germany, Massachusetts General Hospital, Harvard Medical School, Charlestown, Massachusetts 02129, Department of Medical Biochemistry, University of Aarhus, 8000 Aarhus C, Denmark, Department of Pathology and Centre for Neurosciences, The University of Melbourne, Victoria 3010, Australia, The Mental Health Research Institute of Victoria, Parkville, Victoria 3052, Australia, and Biota Structural Biology Laboratory, St. Vincent's Institute of Medical Research, 41 Victoria Parade, Fitzroy, Victoria 3065, Australia

Received October 18, 2005; Revised Manuscript Received January 6, 2006

ABSTRACT: SorLA/LR11 is a sorting receptor that regulates the intracellular transport and processing of the amyloid precursor protein (APP) in neurons. SorLA/LR11-mediated binding results in sequestration of APP in the Golgi and in protection from processing into the amyloid-β peptide (Aβ), the principal component of senile plaques in Alzheimer's disease (AD). To gain insight into the molecular mechanisms governing sorLA and APP interaction, we have dissected the respective protein interacting domains. Using a fluorescence resonance energy transfer (FRET) based assay of protein proximity, we identified binding sites in the extracellular regions of both proteins. Fine mapping by surface plasmon resonance analysis and analytical ultracentrifugation of recombinant APP and sorLA fragments further narrowed down the binding domains to the cluster of complement-type repeats in sorLA that forms a 1:1 stoichiometric complex with the carbohydrate-linked domain of APP. These data shed new light on the molecular determinants of neuronal APP trafficking and processing and on possible targets for intervention with senile plaque formation in patients with AD.

SorLA/LR11 (hereafter referred to as sorLA) is a 250 kDa type 1 transmembrane protein highly expressed in neurons of the cortex and hippocampus (*1*, *2*). It is a mosaic receptor that shares structural similarities both with a family of the vacuolar protein sorting 10 protein (Vps10p)[1] domain containing receptors that act in intracellular protein trafficking (*3*) and with the low-density lipoprotein receptor (LDLR) gene family of endocytic receptors (*4*, *5*). SorLA is synthesized as a pre-proprotein with a 53 amino acid propeptide (pro-LA) that is cleaved in the secretory pathway of the cell by furin. Cleavage of the propeptide is an important step in the maturation process of the receptor and is essential to activate its ligand binding competence (*6*). Apart from the propeptide, the luminal domain of mature sorLA consists of the Vps10p domain, β-propeller and epidermal growth factor (EGF) domains, and a cluster of 11 complement-type repeat (CR) domains, as well as a cassette of six fibronectin (FN) type III domains (*7*). Similar to related receptors of the Vps10p domain and LDLR gene families, sorLA seems to be a multifunctional protein engaged in a number of cellular activities including intracellular protein transport, endocytosis, and signal transduction. For example, sorLA has been shown to act as a receptor for lipoproteins (*8*), platelet-derived growth factor (PDGF) BB (*9*), and glia-derived neurotrophic factor (GDNF) (*10*) and to affect proliferation and migration of smooth muscle cells (*11*−*13*).

Recently, we have uncovered a novel surprising function for sorLA as a regulator of processing of the amyloid precursor protein (APP) and as a potential risk factor for spontaneous Alzheimer's disease (AD) (*14*). AD is the most common neurodegenerative disorder of modern societies and accounts for 50−60% of all age-related dementia. The disease afflicts 8−10% of the population over age 65 and almost 50% when age is above 85 (*15*, *16*). One of the main pathological hallmarks of AD is the accumulation of extra-

[†] This work was funded in part by grants from the DFG and BMBF (to T.E.W.), the Lundbeck Foundation, the American Health Assistance Foundation, and the Danish Medical Research Council (to O.M.A.), the NIH (to B.T.H.), and The National Health and Medical Research Council of Australia (to C.L.M., M.W.P., W.J.M., and R.C.).

* Address correspondence to this author. Tel: +49-30-9406-3749. Fax: +49-30-9406-3382. E-mail: o.andersen@mdc-berlin.de.

[‡] Max-Delbrueck-Center for Molecular Medicine.

[§] Massachusetts General Hospital, Harvard Medical School.

[||] University of Aarhus.

[⊥] Department of Pathology, The University of Melbourne.

[#] The Mental Health Research Institute of Victoria.

[△] St. Vincent's Institute of Medical Research.

[◇] Centre for Neurosciences, The University of Melbourne.

[1] Abbreviations: AD, Alzheimer's disease; APP, amyloid precursor protein; Aβ, amyloid-β peptide; pro-LA, sorLA propeptide (residues 1−53); Vps10p, vacuolar protein sorting 10 protein; PAGE, polyacrylamide gel electrophoresis; FLIM, fluorescence lifetime imaging microscopy; FRET, fluorescence resonance energy transfer; RAP, receptor-associated protein; MESD, mesodermal development; CR domain, complement-type repeat domain; LDLR, low-density lipoprotein receptor; LRP1, LDLR-related protein-1; FN, fibronectin: PCR, polymerase chain reaction; KPI, Kunitz proteinase inhibitor; GFD, growth factor-like domain; EGF, epidermal growth factor; RU, response units; GDNF, glia-derived neurotrophic factor; PDGF, platelet-derived growth factor.

10.1021/bi052120v CCC: $33.50
Published on Web 02/04/2006

cellular deposits of an amyloid-β peptide (Aβ) that is derived from proteolytic processing of APP in neurons. Because deposition of Aβ plays a decisive role in onset and progression of AD, much attention has been focused on delineating the normal pathway by which APP molecules are proteolytically processed into Aβ as well as the pathological alterations leading to increased amyloid peptide formation in patients with AD (*17*). Because the production of Aβ is strongly dependent on the intracellular fate of APP, it is believed that mislocalization of the precursor results in abnormal processing and enhanced Aβ production that subsequently leads to an early onset of AD.

APP follows a complex intracellular trafficking pathway that influences processing to either a soluble fragment, sAPPα (nonamyloidogenic), or sAPPβ and the insoluble Aβ (amyloidogenic). En route through the secretory pathway to the cell surface, most newly synthesized APP molecules are cleaved into sAPPα by α-secretase while some precursor molecules are reinternalized from the plasma membrane and delivered to endocytic compartments for β-secretase (and subsequent γ-secretase) processing into sAPPβ and Aβ (*18*, *19*). Accordingly, the intracellular transport and subcellular localization of APP are crucial determinants of processing and Aβ generation. We demonstrated previously that sorLA acts as a neuronal sorting receptor for APP that interacts with the precursor protein in vitro and in living cells. SorLA activity in neurons causes sequestration of APP in the Golgi and decreased processing, whereas ablation of sorLA expression in knockout mice results in increased levels of Aβ in the cerebral cortex (*14*). The physiological role of sorLA in Aβ production and AD progression is underscored by the lack of receptor expression in the brain of patients suffering from AD (*14*, *20*).

Here, we have delineated the exact binding sites that are responsible for the interaction of APP and sorLA in neurons, and we have characterized their mode of action as a first approach toward elucidating this novel molecular mechanism that controls APP trafficking and processing in the brain.

EXPERIMENTAL PROCEDURES

Recombinant Protein Production. Recombinant RAP was produced according to described protocols (*21*). For production of recombinant MESD, the fragment coding amino acid residues 30−224 was amplified by PCR from the cDNA of murine MESD (kindly provided by J. Herz, University of Texas Southwestern Medical Center) using the primer pair 5′-GCC CAT ATG GCG GAC ACT CCG GGC GAG GCC ACC CC-3′ and 5′-GCC CTC GAG CTA AAG GTC TTC TCT TCT GCT CCC AGC-3′ and cloned into the pET-16b vector (Novagen). The protein was expressed in *Escherichia coli* line BL21/DE3 pLysS and purified by conventional Ni^{2+}-ion chelation chromatography. For removal of the His_6 tag, the protein was incubated with factor Xa for 16 h at 4 °C, and the enzyme was subsequently removed using the factor Xa removal kit (Sigma) (O. M. Andersen, manuscript in preparation).

The sorLA fragments comprising residues 54−2107 (extracellular domain) or residues 54−731 (Vps10p domain) were generated as previously described (*6*). For additional sorLA fragments, we constructed EBNA 293 expression vectors as follows. A cDNA coding for the human *sorLA* gene was used as the PCR template to generate *Nhe*I−*Not*I fragments encoding the sorLA β-propeller and EGF domains (residues Glu^{728}−Thr^{1049}) by the primer pair 5′-GC CCG CTA GCA GAA GAG AAC GAG TTC ATT CTG TAT GC-3′ and 5′-GC GGC CGC TCA GGT GTT CTC TTC TTT GAC ACA GG-3′ and the sorLA CR cluster (residues Val^{1044}−Thr^{1526}) by the primer pair 5′-GC CCG CTA GCT GTC AAA GAA GAG AAC ACC TGT CTT CGC-3′ and 5′-GC GGC CGC TCA AGT CAA CTC ATC ACT GCA GGC C-3′, as well as a fragment spanning both regions (residues Glu^{728}−Thr^{1526}) by the primer pair 5′-GC CCG CTA GCA GAA GAG AAC GAG TTC ATT CTG TAT GC-3′and 5′-GC GGC CGC TCA AGT CAA CTC ATC ACT GCA GGC C-3′. After ligation of PCR products into pGemTeasy (Promega), the fragments were verified by sequencing. The coding fragments were cut out by *Nhe*I and *Not*I digests and inserted into the eukaryotic expression vector pCepPu-sp-his-myc-fXa as described previously (*22*). The expression vectors were introduced into EBNA 293 cells to generate cell clones that secrete large amounts of the recombinant receptor fragments. The conditioned cell medium was harvested after 48 h of cultivation, and the proteins were purified as previously described (*22*).

The recombinant fragments of the human APP_{695} protein were generated as follows. d1 (APP28−123) and d2 (APP124−189) were expressed and purified from *Pichia pastoris* as previously described (*23*, *24*). d2d3d6 (APP124−624) was also expressed in *P. pastoris* by amplifying the DNA encoding APP124−624 with the primers 5′-GCT CGA GAA AA GAG AGGCTA GTG ATG CCC TTC TCG-3′ and 5′-CCC GGG TTA TTT GTT TGA ACC CAC ATC TTC TGC-3′ and cloned into pIC9 as an *Xma*I fragment. The recombinant APP fragment was expressed as a secreted protein and purified from the media by heparin chromatography on a heparin−hyperD column (1.6 × 12 cm; Biosepra S.A.) followed by anion-exchange on a QhyperD column (4.6 × 100 mm; Biosepra S.A.). d1d2d3d6 (APP28−624) was similarly expressed in *P. pastoris* by amplifying the DNA encoding APP28−624 with the primers 5′-GGT CGA CAA AAG AGA GGC TCT GCT GGC TGA ACC CCA GAT TG-3′ and 5′-CCC GGG TTA TTT GTT TGA ACC CAC ATC TTC TGC-3′ and cloned into pIC9 as an *Xma*I fragment. The secreted d1d2d3d6 was purified from the media under similar conditions as for d2d3d6 by heparin and anion-exchange chromatography. d6A (APP316−498) was expressed in *E. coli* by amplifying the DNA encoding APP316−498 with the primers 5′-CGC ATA TGT TCC AGA AAG CCA AAG AGA G-3′ and 5′-CCA AGC TTC ATG AAT AGT TTT GCT CTT TCT G-3′ and cloning into *Nde*I−*Hin*dIII-digested pRESTA (Invitrogen). The d6A expressing cells were induced with IPTG and purified from the cell lysate by heparin and anion-exchange chromatography as for the other fragments.

Surface Plasmon Resonance Analysis. For immobilization of sorLA fragments, the recombinant proteins were dialyzed against a sodium acetate, pH 4.0, buffer and coupled to CM5 chips (BIAcore) at a concentration of 10 μg/mL after activation using a 1:1 mixture of 0.2 M *N*-ethyl-*N*-[3-(dimethylamino)propyl]carbodiimide and 0.05 M *N*-hydroxysuccinimide in water. The remaining binding sites were blocked with 1 M ethanolamine, pH 8.5. Approximately 60 fmol/mm^2 sorLA was immobilized. The sample and running

buffer was 10 mM HEPES, pH 7.4, 150 mM NaCl, 5 mM $CaCl_2$, and 0.005% Tween 20. Regeneration of the chip surface was performed by alternating 10 μL pulses of regeneration buffer (10 mM glycine hydrochloride, pH 4.0, 20 mM EDTA, 500 mM NaCl, and 0.005% Tween 20) and 0.01% SDS. All measurements were conducted on a BIAcore2000 instrument.

Analytical Ultracentrifugation. Molecular mass determination and analysis of complex formation were performed using the sedimentation equilibrium technique in an analytical ultracentrifuge, XL-A (Beckman). Approximately 70 μL of protein samples in 10 mM HEPES, pH 7.4, 150 mM NaCl, and 5 mM $CaCl_2$ was centrifuged in six-channel cells for 2 h at 20000*g* followed by 36−38 h equilibrium speed at 11300*g* at 10 °C in an An-60 Ti rotor. The radial absorbance distributions at sedimentation equilibrium were recorded at different wavelengths and fitted globally using the program POLYMOLE (*25*). To determine complex stoichiometry, various amounts of APP d6A were added to a 1 μM sorLA CR cluster solution and analyzed with respect to weight-average molecular masses (M_w).

Fluorescence Lifetime Imaging Microscopy (FLIM) Assay. FLIM has been recently described as a novel technique for the analysis of protein proximity (*26*, *27*). The technique is based on the fact that fluorescence lifetime of a donor fluorophore shortens in the presence of a fluorescence resonance energy transfer (FRET) acceptor in close proximity, less than 10 nm. Immunostaining of transfected N2a cells was done after cells were fixed in 4% paraformaldehyde and permeabilized by 0.5% Triton X-100. Cells were immunostained for APP_{695} by monoclonal antibody 8E5 (raised against residues 444−592 of APP_{770}, a gift from Elan Pharmaceuticals) and for $sorLA^{wt}$ or $sorLA^{\Delta CD}$ by rabbit amino-terminal anti-soluble sorLA antibody. APP_{695} was labeled by the donor fluorophore Alexa488-conjugated secondary antibody (Molecular Probes) and sorLA constructs by the acceptor fluorophore Cy3-conjugated antibody (Jackson Immunoresearch). Immunostained cells were mounted for confocal or two-photon microscopic imaging. For the FLIM measurement, a mode-locked Ti-sapphire laser (Spectra Physics) sends a 100 fs pulse every 12 ns to excite the donor fluorophore at 800 nm, and a high-speed MCP5900 detector (Hamamatsu) was used to measure fluorescence lifetimes. Images were acquired using a Bio-Rad Radiance 2000 multiphoton microscope. We imaged whole cells using the 60× objective, and the num.apertus value was set to 1.20. All of the flurophore lifetimes were collected in the 0−2500 ps range with the threshold set to 50 counts. Donor fluorophore lifetimes were fit to two exponential decay curves to calculate within each pixel the interaction with the acceptor fluorophore by software from Becker and Hickel. Statistical testing was performed by Student's *t* test.

Confocal Immunofluorescence Microscopy. SH-SY5Y cells were plated on glass coverslips coated with 0.1% gelantine/PBS and left overnight. Cells were cotransfected with APP_{695} and wild-type sorLA or mutant $sorLA^{\Delta CD}$ in a ratio of 1:1, respectively, to a total amount of 1 μg of cDNA per 24 wells and 3 μL of FuGENE 6 (Roche) per well in OPTIMEM. After 48 h cells were washed with PBS and fixed in 4% paraformaldehyde for 10 min, washed again, and permeabilized and blocked for 1 h in 0.3% Triton X-100, 0.2% BSA, and 10% serum in PBS (for cell surface staining without Triton X-100). Cells were incubated overnight at 4 °C with a goat antiserum against the extracellular part of sorLA (1:500) and monoclonal mouse antibody 6E10 against the luminal part of APP (1:500) in PBS. Coverslips were washed five times in PBS and incubated for 4 h at room temperature with secondary antibodies Alexa555 donkey anti-mouse IgG conjugates (1:500; Molecular Probes) and Alexa488 donkey anti-goat IgG conjugates (1:500; Molecular Probes). Coverslips were washed five times with PBS and mounted on glass slides with Dako mounting medium. Confocal images were obtained using a Zeiss confocal microscope (100× lens), and images were processed with an LSM 5 image browser.

RESULTS

The Extracellular Domain of SorLA Is Sufficient for Interaction with APP in Vivo. Conceivably, association of APP with sorLA in vivo may take place via contacts in the extracellular and/or the cytoplasmic domains of both proteins similarly to previously described modes of interaction of APP with the LDLR-related protein-1 (LRP1) (*28*, *29*). To establish the relevance of extra- and intracellular sorLA domains for interaction in cells, we transfected human neuronal SH-SY5Y cells with expression vectors for full-length sorLA ($sorLA^{wt}$) or a mutant receptor that lacks the cytoplasmic tail ($sorLA^{\Delta CD}$). The integrity of the two polypeptides was confirmed by Western blot analysis (Figure 1A). In line with the expected expression domains, antibodies directed against the extracellular sorLA region detected protein bands of similar intensity in $sorLA^{wt}$ and $sorLA^{\Delta CD}$ expressing SH-SY5Y cells while an antiserum against the carboxyl-terminal domain only recognized the full-length protein. Colocalization of both receptor variants with APP was tested by confocal immunofluorescence microscopy after cotransfection with an APP_{695} construct. No difference between the localization pattern of overexpressed APP (this study) and endogenous APP (*14*) could be identified. In the presence of $sorLA^{wt}$, APP mainly localized to intracellular compartments, in particular in the perinuclear region where it colocalized with full-length sorLA in some vesicles (Figure 1B). Because the anti-APP antibody (6E10) recognizes the luminal part of APP, immunoreactivity may represent both the full-length membrane-anchored precursor as well as APP processing products trapped in the cells. Predominant intracellular localization of APP and sorLA was confirmed by the complete absence of immunoreactivity on the cell surface in cells not permeabilized prior to antibody incubation (Figure 1B). In contrast to $sorLA^{wt}$, $sorLA^{\Delta CD}$ showed a distinct localization at the cell surface in the absence of permeabilization (Figure 1C), indicating that the lack of sorting signals of the cytoplasmic tail enhances shunt of the receptor to the plasma membrane. The subcellular pattern of $sorLA^{\Delta CD}$ was paralleled by partial redistribution of coexpressed APP_{695} to the cell surface (Figure 1C) as clearly seen when cells were stained for surface proteins in the absence of detergent. These findings confirmed previous observations for Chinese hamster ovary cells (*14*) in a cellular model more relevant to AD. Whether $sorLA^{\Delta CD}$ is directly involved in active transport of APP to the cell surface or merely acts as a retention molecule for the precursor in this compartment remains to be elucidated.

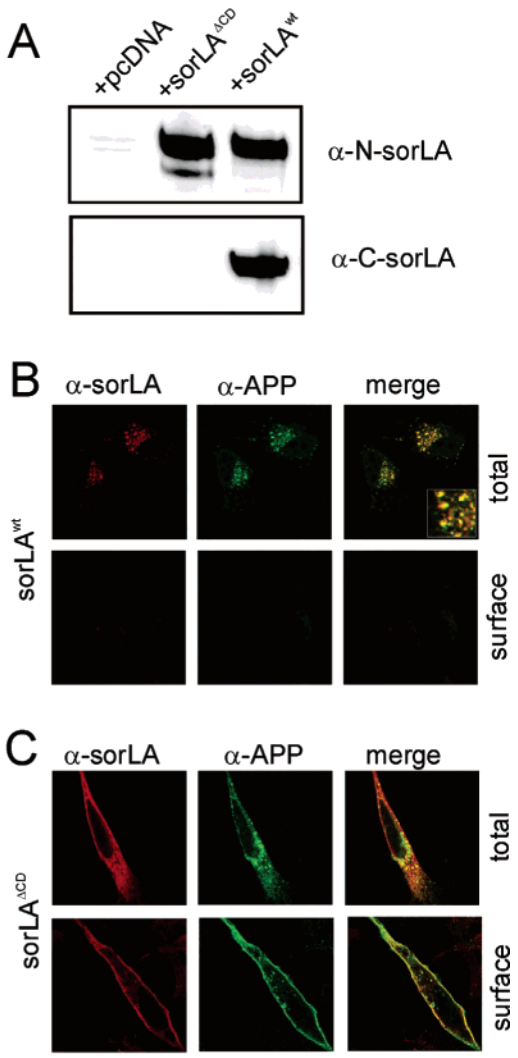

FIGURE 1: Colocalization of APP with the extracellular domain of sorLA in SH-SY5Y neurons. SH-SY5Y cells were cotransfected with expression constructs for APP_{695} and wild-type sorLA (sorLA^{wt}) or a mutant that lacks the cytoplasmic tail (sorLA$^{\Delta CD}$). (A) Integrity of the sorLA polypeptides was verified by Western blot analysis in cell lysates using antibodies directed against the amino terminus of sorLA (upper panel) or the carboxyl terminus present in sorLA^{wt} but not sorLA$^{\Delta CD}$ (lower panel). (B) Confocal immunofluorescence microscopy demonstrates colocalization of APP and sorLA^{wt} in the perinuclear region of SH-SY5Y cells permeabilized with detergent (B, total) but not on the plasma membrane of nonpermeabilized cells (B, surface). The inset shows perinuclear vesicles that contain both sorLA and APP at higher magnification. (C) Colocalization of APP and sorLA$^{\Delta CD}$ on the cell surface of permeabilized (C, total) a well as nonpermeabilized cells (C, surface).

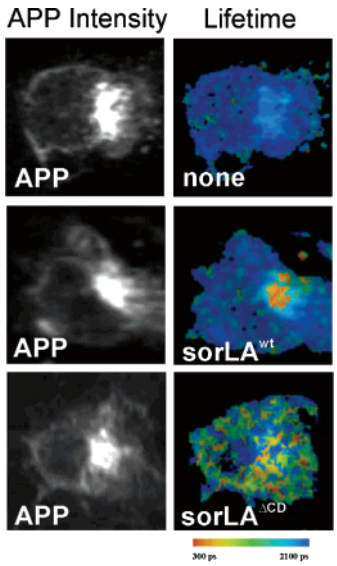

FIGURE 2: FLIM analysis of the interaction of APP with the extracellular domain of sorLA in N2a cells. Mouse neuronal N2a cells were transfected with expression constructs for APP_{695} (upper panel), APP_{695} and sorLA^{wt} (middle panel), or APP_{695} and sorLA$^{\Delta CD}$ (lower panel). Twenty-four hours later, the cells were fixed and immunostained with a Alexa488-labeled anti-APP antibody as donor fluorophore in either the absence (upper panel) or presence of a Cy3-labeled anti-sorLA antibody as acceptor fluorophore (center and lower panels). The figures display intensity images of APP (left) and pseudocolored FLIM images (right) indicating shortening of lifetime from blue (no FRET) to orange/red color (with FRET). In the absence of the acceptor (upper panel), the Alexa488 lifetime on APP was 2028 ps and appeared as pseudocolored blue. In the presence of sorLA^{wt} and sorLA$^{\Delta CD}$, donor lifetimes were markedly shortened (1734 and 1543 ps, respectively), appearing pseudocolored red.

Table 1: FLIM Analysis of the Interaction of SorLA^{wt} and SorLA$^{\Delta CD}$ with APP[a]

donor	acceptor	lifetime (ps) (mean ± SD)	*n* (cells)	significance
APP_{695}-myc (Alexa488)	none	2034 ± 45	7	−
		2028 ± 20	9	−
		2025 ± 30	9	−
APP_{695}-myc (Alexa488)	sorLA$^{\Delta CD}$ (Cy3)	1364 ± 257	7	$P < 0.001$
		1543 ± 262	8	$P < 0.001$
		1596 ± 258	9	$P < 0.001$
APP_{695}-myc (Alexa488)	sorLA^{wt} (Cy3)	1734 ± 185	9	$P < 0.001$

[a] Determination of FLIM of the donor fluorophore Alexa488 on APP in the absence or presence of the acceptor fluorophore Cy3 on sorLA^{wt} or sorLA$^{\Delta CD}$. The statistical significance was evaluated by Student's *t* test, where *n* equals the number of cells quantified.

Because colocalization studies have a spatial resolution of >250 nm, we used fluorescence lifetime imaging microscopy (FLIM) to confirm the interaction of sorLA and APP in the presence or absence of the receptor tail. FLIM is based on the observation that the lifetime of a donor fluorophore is shortened in the presence of a fluorescence resonance energy transfer (FRET) acceptor in close proximity (<10 nm) (*27*). Accordingly, we transfected murine neuronal N2a cells with APP_{695} and wild-type sorLA constructs and immunostained the cells with 8E5 antibody against the amino terminus of APP (N-APP) labeled by Alexa488 and with a Cy3-labeled acceptor antibody against the amino terminus of sorLA. In the absence of an acceptor fluorophore in control cells, the donor lifetime on N-APP was 2028 ps (Figure 2, Table 1). Immunostaining of sorLA^{wt} with the Cy3-labeled acceptor antibody shortened the donor lifetime significantly to 1734 ± 185 ps ($P < 0.001$), indicating close contact, especially in the perinuclear (Golgi) region. When cells coexpressed APP and sorLA$^{\Delta CD}$, a similar decrease in donor lifetime on N-APP to 1543 ± 262 ps ($P < 0.001$) was observed (Figure 2, Table 1). However, shortening of lifetime appeared in a scattered pattern across the cell surface rather than in the perinuclear region, in line with the altered subcellular distribution of sorLA$^{\Delta CD}$ compared to sorLA^{wt}. From these studies we concluded that the extracellular (ectodomain) of sorLA is sufficient for interaction with APP

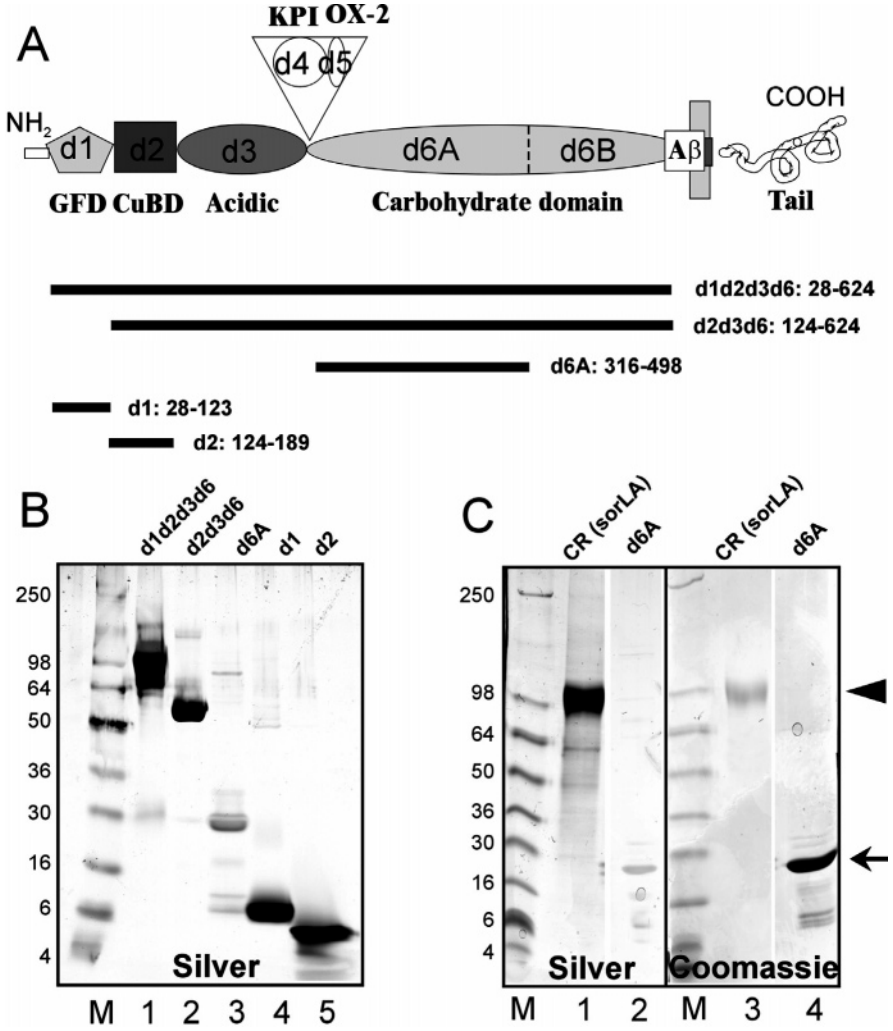

FIGURE 3: Schematic representation and generation of truncated APP domains. (A) Domain assembly of the APP polypeptide chain, including an amino-terminal growth factor-like region (GFD), a Cu^{2+} binding domain (CuBD), an acidic region, and the carbohydrate domain (d6) which is composed of two regions (d6A and d6B) modified by glycosylation. The transmembrane domain is indicated and is followed by the cytoplasmic domain (Tail). Also depicted are the Kunitz proteinase inhibitor domain (KPI) and the OX-2 homology region, but these domains are removed by splicing of the neuronal variant of APP. The extensions of the produced APP fragments are indicated below the APP polypeptide chain by horizontal lines and by amino acid numbers. (B) Silver-stained SDS−PAGE analysis of 15 μg of purified APP domains used for binding studies: lane M (molecular markers, M_w, are provided to the left of the panel), lane 1 (d1d2d3d6, residues 28−624), lane 2 (d2d3d6, residues 124−624), lane 3 (d6A, residues 316−498), lane 4 (d1, residues 28−123), and lane 5 (d2, residues 124−189). Residue numbers are provided according to APP_{695} numbering. (C) Comparison by SDS−PAGE analysis of staining properties of the d6A fragment (arrow), compared to a fragment from sorLA comprising the CR cluster (arrowhead) using silver nitrate or Coomassie.

in neurons and that this interaction influences intracellular localization of the precursor protein.

Identification of the SorLA Binding Region in APP. The neuronal variant of APP is a 695 amino acid residue polypeptide that harbors a large extracellular domain composed of multiple structural elements (Figure 3A) including (from amino to carboxyl terminus) a growth factor-like domain (GFD, d1; structure presented in ref *30*), a copper binding domain (CuBD, d2; structure presented in ref *24*), an acidic region known to undergo phosphorylation (acidic domain, d3), a carbohydrate-linked domain (d6; structures presented in refs *31* and *32*), and the Aβ that is partly inserted in the transmembrane region of the protein. In addition, larger APP variants such as APP_{770} include a Kunitz proteinase inhibitor domain (KPI, d4) and an OX-2 homology region (d5). Previously, we have shown that the ectodomains of APP_{695} and APP_{770} bind to sorLA in vitro with similar affinities, indicating that neither d4 (KPI) nor d5 (OX-2) constitutes the sorLA binding region (*14*). To resolve which of the common APP domains, d1, d2, d3, and/or d6, are responsible for sorLA binding, we expressed them as single APP domains (d1, d2, d6) or as a larger fragment comprising domains d2, d3, and d6 (d2d3d6). All fragments were produced in either *E. coli* or *P. pastoris* and purified to homogeneity as seen by SDS−PAGE analysis (Figure 3B). The weaker signal intensity observed for the d6A fragment in this experiment was an artifact of silver nitrate staining and was not seen when the protein domains were labeled with Coomassie (Figure 3C).

Surface plasmon resonance analysis was used to evaluate the interaction of the purified APP fragments with the sorLA ectodomain immobilized on the biosensor chip surface (Figure 4A). The functional integrity of the sorLA polypeptide on the chip surface was verified by demonstrating its ability to bind previously described ligands for sorLA, including the receptor-associated protein (RAP, not shown) and PDGF-BB (*9*) (Supporting Information, Figure 1A). In these studies, APP fragments d1, a fragment spanning most

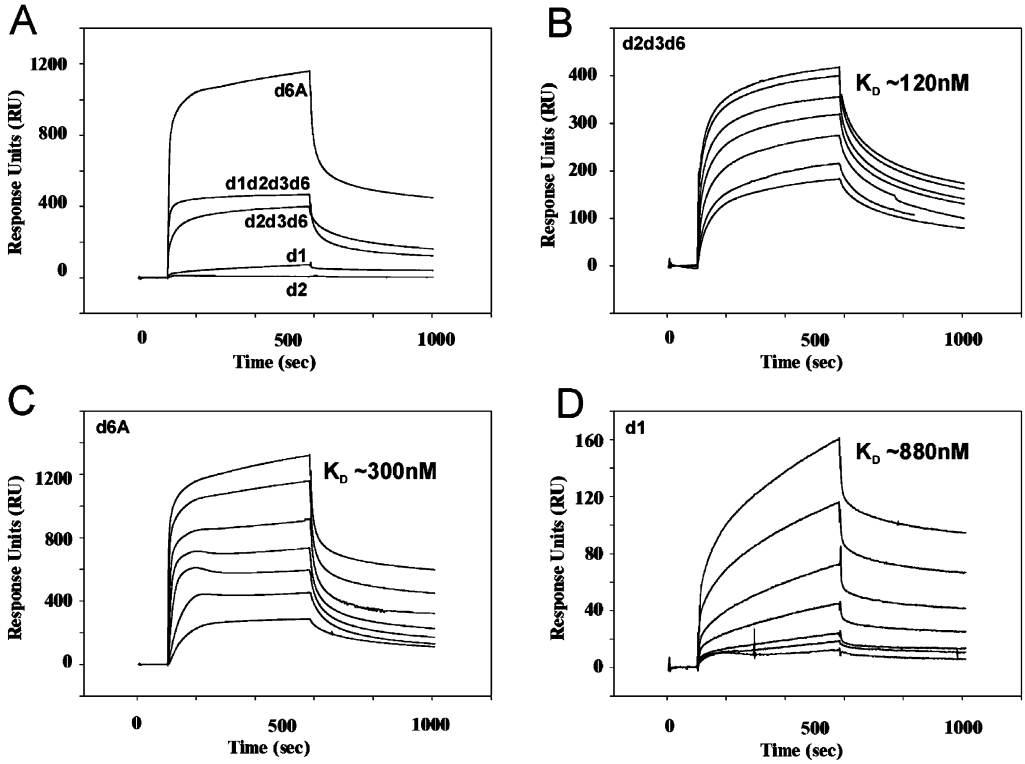

FIGURE 4: Surface plasmon resonance analysis of binding of APP domains to sorLA. (A) The curves represent binding of identical concentrations (5 μM) of APP domains d1d2d3d6, d2d3d6, d6A, d2, and d1 to the sorLA ectodomain immobilized on the BIAcore sensor chip. (B−D) For estimation of binding kinetics, a concentration series of fragments d2d3d6 (B), d6A (C), and d1 (D) at 0.1, 0.2, 0.5, 1.0, 2.0, 5.0, and 10 μM were applied to the sorLA biosensor. The binding dissociation constants (K_D) as estimated using the BIAevaluation software are provided in Table 2A.

Table 2: Kinetic Parameters for Binding of APP Fragments to the Immobilized Ectodomain (A) or CR Cluster (B) of SorLA[a]

	k_a (1/M s)	k_d (1/s)	K_A (1/M)	K_D (M)
	(A) Full-Length SorLA			
d1d2d3d6[b]	4.9×10^4	4.1×10^{-3}	1.2×10^7	8.4×10^{-8}
d2d3d6	1.5×10^4	1.8×10^{-3}	8.1×10^6	1.2×10^{-7}
d1	4.7×10^2	4.5×10^{-4}	1.3×10^6	8.8×10^{-7}
d2		no binding observed		
d6A	1.7×10^3	5.2×10^{-4}	3.3×10^6	3.0×10^{-7}
	(B) Isolated SorLA CR cluster			
d6A	3.4×10^3	1.1×10^{-3}	3.0×10^6	3.4×10^{-7}

[a] All parameters were determined using the BIAevaluation 3.1 software and fitting using the 1:1 Langmuir binding equation. [b] Data from sensorgrams in ref *14*.

but not the entire d6 (called d6A, Figure 3A), and d2d3d6 fragments all bound to sorLA whereas d2 showed no detectable interaction, even when tested at very high concentrations (50 μM; data not shown). As an additional control for the specificity of the interaction, we showed that the association between immobilized sorLA and d1d2d3d6 was abolished by EDTA (Supporting Information, Figure 1C), a hallmark of Ca^{2+}-dependent binding of ligands to lipoprotein receptors. Application of a concentration series of APP fragments (Figure 4B-D) and fitting of the corresponding binding curves demonstrated that the native APP_{695} ectodomain (d1d2d3d6) (*14*) and fragment d2d3d6 (Figure 4B) bound with similar dissociation constants of $K_D \sim 84$ nM and $K_D \sim 120$ nM, respectively (Figure 4, Table 2A). Fragment d6A showed comparable binding ($K_D \sim 300$ nM) (Figure 3C, Table 2A). The d1 of APP also associated with sorLA albeit with significantly lower affinity of $K_D \sim 880$ nM (Figure 3D, Table 2A). Taken together, these experiments identified two independent sorLA binding sites within APP, one located in the carboxyl-terminal carbohydrate-linked domain (d6) and one in the amino-terminal growth factor-like region (d1).

Domains d1 and d6 Bind to the Same Site on SorLA. To test whether d1 and d6 might bind simultaneously to sorLA and thereby work cooperatively to generate a single high-affinity interaction site or whether they compete for the same binding region, we performed competition binding analysis using BIAcore. Precoating of sorLA on the sensor chip with d1 (10 μM) did not block binding of d2d3d6. Rather, d2d3d6 easily displaces prebound d1 when applied at 1 μM, suggesting that the two sites compete for an identical recognition motif (Figure 5A). Complete inhibition of d1 binding by prebinding of d2d3d6 to sorLA provided further proof of such a model (Figure 5B). These observations are in agreement with the determined kinetic parameters (Table 2A) for the isolated domain interactions where the association rate constant for d1 is much slower than for d6 (in d2d3d6) and, therefore, likely explains why d1 is competed out by the simultaneous addition of d1 and d2d3d6. In conclusion, these data provided evidence for two competing sorLA binding sites, d1 and d6, in the APP ectodomain.

The Vps10p Domain Does Not Interact with APP. Next, we sought to identify the region in sorLA (schematic representation in Figure 8) that mediates the association with APP. Initially, we focused our attention on the Vps10p domain of the receptor that has been shown to bind several ligands, e.g., RAP (*6*) and GDNF (*10*). Because binding of ligands to the Vps10p domain is blocked by the receptor's

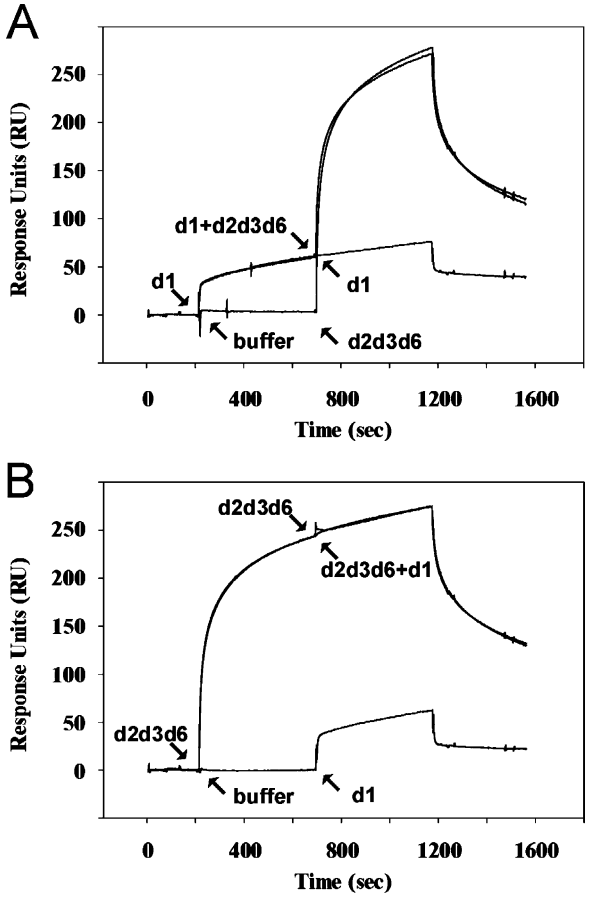

FIGURE 5: Binding of d2d3d6 displaces d1 from sorLA. (A) At 200−700 s, immobilized sorLA was precoated with d1 (10 μM), resulting in 80 response units (RU). Subsequent addition of a 10:1 mixture of d1 (10 μM) and d2d3d6 (1 μM) to the flow cell (at 700 s) resulted in a further increase to 280 RU, indicating unimpaired binding of d2d3d6 to the receptor in the presence of a molar excess of d1. As control, addition of d1 (at 700 s) to the precoated receptor did not result in a further increased response, demonstrating complete saturation of the receptor with d1. Identical RU for d2d3d6 binding to d1-coated or buffer-treated sorLA (at 700 s) suggest displacement of prebound d1 by d2d3d6. (B) Precoating of immobilized sorLA with d2d3d6 (at 200−700 s) blocks further association with d1 (10 μM) applied together with d2d3d6 (1 μM) at 700 s. For comparison, the increase in response caused by injection of d1 (at 700 s) to buffer-treated sorLA is shown (~60 RU).

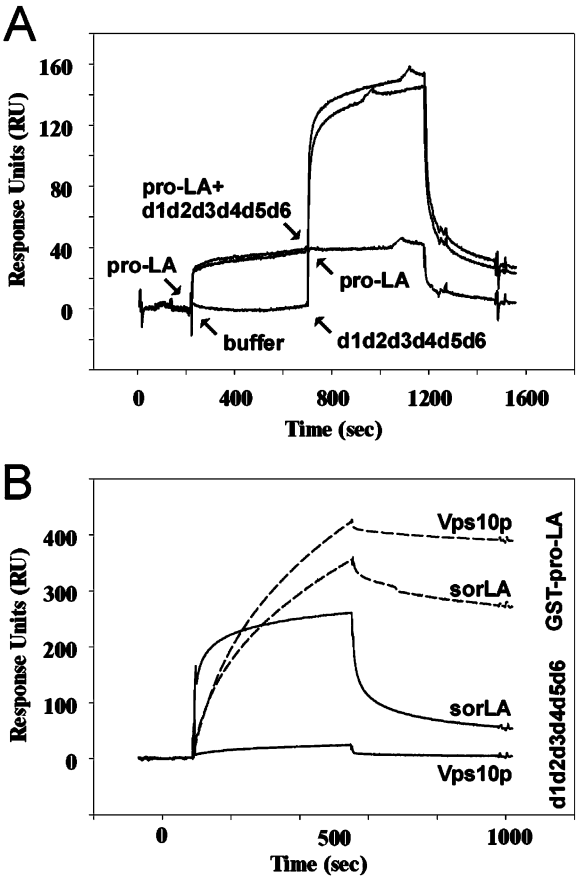

FIGURE 6: Interaction between APP and sorLA is not mediated by the Vps10p domain. (A) Precoating of immobilized sorLA with 1 μM sorLA propeptide (pro-LA) at 200−700 s does not inhibit subsequent association with APP domain d1d2d3d4d5d6 (1 μM) when a 1:1 mixture of pro-LA and d1d2d3d4d5d6 is applied at 700 s. As control, addition of pro-LA (at 700 s) to the precoated receptor did not result in a further increased response, demonstrating complete saturation of the Vps10p domain of the receptor. For comparison, binding of d1d2d3d4d5d6 (at 700 s) to the buffer-treated receptor is shown. (B) Comparative binding of 1 μM d1d2d3d4d5d6 (solid lines) and GST-pro-LA (broken lines) to the ectodomain or the isolated Vps10p domain of sorLA immobilized on the biosensor.

propeptide (pro-LA) (*6*), we tested whether pro-LA would inhibit the association of sorLA with the ectodomain of APP_{770} (d1d2d3d4d5d6). Remarkably, precoating of the Vps10p domain by the pro-LA had no effect on the interaction between immobilized sorLA and APP (Figure 6A). This finding was corroborated by the lack of binding of d1d2d3d4d5d6 to the isolated Vps10p domain on a BIAcore chip (Figure 6B). As a control for the functional integrity of the immobilized Vps10p domain, we showed efficient binding of a GST-pro-LA fusion protein (Figure 6B). Accordingly, we conclude that the sorLA Vps10p domain is not able to bind APP.

Binding of APP to the LDLR Homology Region in SorLA. Since the Vps10p domain was not involved in recognition of APP, we tested structural elements in sorLA shared with members of the LDLR gene family, namely, the β-propeller, the EGF domain, and the cluster of 11 CR domains. Commonly, mapping of ligand binding to these receptors has been carried out by competition assays applying RAP, an endoplasmic reticulum-resident chaperone that blocks association of ligands with CR domains (*21*, *33*). More recently, a second chaperone (MESD) has been described (*34*, *35*) that interferes with the ligand binding properties of the β-propeller and EGF domains (*36*, *37*). Thus, we reasoned that, by combination of the two antagonists, we might be able to dissect whether APP binds any of these elements in sorLA. Prebinding of RAP to sorLA almost completely inhibited the interaction with d2d3d6 of APP (Figure 7A) whereas MESD had no effect as both proteins, MESD and d2d3d6, concurrently bound to sorLA (Figure 7B). In summary, this pattern of inhibition suggests that APP associates specifically with the string of CR domains in sorLA.

Stoichiometric Complex Formation between d6A and the CR Cluster of SorLA. To extend our fine mapping efforts, we produced truncated fragments of the sorLA ectodomain harboring either the β-propeller followed by the EGF domain (β + E), the isolated CR cluster (CR), or a combination of the two fragments (β + E + CR; see Figure 8A for details).

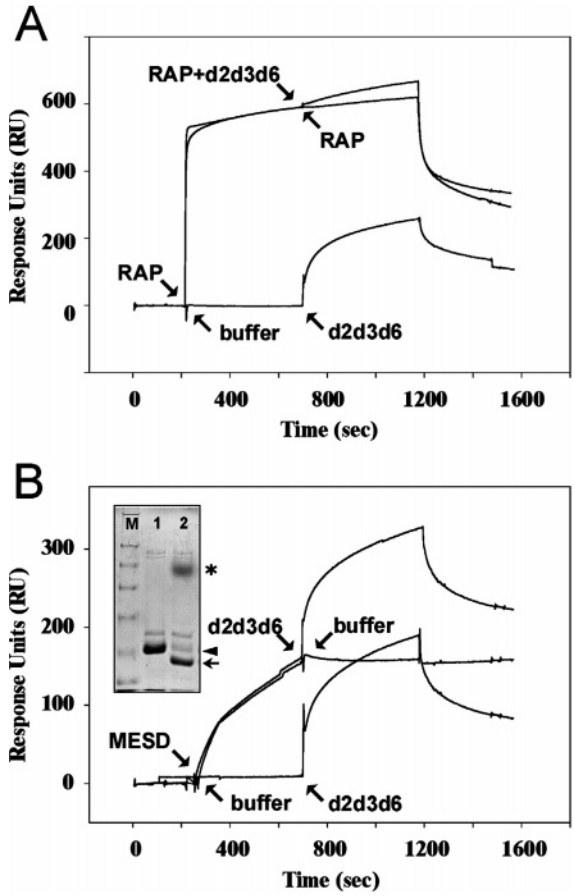

FIGURE 7: RAP but not MESD blocks APP binding to sorLA. (A) Precoating of sorLA with 1 μM RAP (200−700 s) almost completely blocks subsequent binding of 10 μM d2d3d6 (at 700 s). As controls, binding of RAP to RAP-treated receptor and of d2d3d6 to buffer-treated sorLA is shown (at 700 s). (B) Precoating of sorLA with 1 μM MESD (at 200−700 s) has no inhibitory effect on subsequent d2d3d6 binding (injection of 10 μM sample started at 700 s) as documented by a further increase in RU compared to addition of buffer only. As control, binding of d2d3d6 to buffer-treated sorLA (at 700 s) is indicated. (Inset) SDS−PAGE analysis of recombinant MESD before (lane 1, arrowhead) and after cleavage of the His_6 tag (lane 2, arrow) by factor Xa (the trace amount of enzyme that is present in the sample before removal by the factor Xa removal kit is indicated by an asterisk).

All fragments were expressed and purified as intact proteins from EBNA 293 cells using Ni^{2+}-ion chelation chromatography (Figure 8B). When the individual sorLA fragments were immobilized on biosensor chips, no significant interaction with d6A was observed for the isolated β-propeller domain (not shown). In contrast, the CR cluster showed high-affinity binding of d6A (Figure 9A) that could be fitted to a model for a single site interaction with similar kinetic parameters ($K_D \sim 340$ nM) as the interaction between d6A and the entire sorLA ectodomain ($K_D \sim 300$ nM) (Table 2B). To document the presence of a properly folded sorLA CR cluster on the chip surface, we tested the binding of PDGF-BB to this fragment. Although the precise binding site for PDGF-BB on sorLA has so far not been identified, we reasoned that it might be located in the CR domains in line with an established binding site for this ligand on LRP1 (*38*). This hypothesis could be confirmed by demonstration of an identical interaction between PDGF-BB with the entire luminal domain of sorLA as for its isolated CR cluster (Supporting Information, Figure 1B).

Complex formation of APP and sorLA interacting fragments was confirmed by molecular mass determination using the sedimentation equilibrium technique (*25*). When pure preparations of the recombinant domains were characterized by analytical ultracentrifugation, an accurate molecular mass of 21 and 61 kDa for d6A and CR cluster, respectively, was determined (data not shown). When increasing amounts of d6A were titrated into a preparation of the CR cluster, the average molecular mass in the protein mixture increased until the molar ratio of the two fragments equaled 1 (where the equimolar mass is determined to be ~84 kDa, Figure 9B). By the addition of a molar surplus of the d6A no further increase in mass was detected. Rather, the average molecular mass decreased as a result of the addition of the free 21 kDa d6A fragment into the 61 kDa receptor preparation (Figure 9B). This finding is in perfect agreement with the formation of a stable 1:1 stoichiometric complex between d6 in APP and the CR cluster in sorLA.

DISCUSSION

We have characterized the specific binding sites between APP and its neuronal sorting receptor sorLA. This study is of particular interest given the decisive role of the latter in APP proteolytic processing into Aβ in mouse and human (*14*).

Two domains in APP, d1 and d6, were shown to bind overlapping regions in the CR cluster of sorLA. On the basis of the differences in affinities, d6 likely constitutes the preferred binding site and d1 is predicted to play a minor physiological role. This hypothesis is in accordance with the similar affinities determined for d1d2d3d6 and d2d3d6, as d1 has been deleted from the latter construct (see Table 2A) without impacting affinity. Interestingly, the isolated d1 binds with a much slower dissociation rate constant in comparison to the full-length APP ectodomain (that also includes d1), suggesting that, in the context of the entire APP protein, the conformation of the protein may not allow d1 to interact with sorLA.

Because a SPR signal is directly related to the mass of the binding ligand, it was surprising to observe that d6A yielded more than twice the signal of the larger d1d2d3d6 construct. We believe that this might be caused by multimerization of d6A in these experiments, a fact in line with previous observations by Dulubova et al. (*32*). They found that a fragment with almost identical domain boundaries behaved as a monomer at low protein concentrations but formed multimers at high concentration and low salt conditions. To investigate whether the higher response was in fact caused by dimers or higher multimers of d6A, we repeated the binding series of d6A to sorLA in the presence of higher salt buffer (500 mM NaCl versus 150 mM NaCl in the initial experiment). Under these conditions, the response was exactly half of that observed in the low salt experiment (Supporting Information, Figure 1D). These findings confirm a model whereby d6A exists as (at least) a dimeric molecule as previous described by Wang and Ha for a similar fragment of APP (*31*) and where each dimer only can associate with a single sorLA molecule [as is the case for the full-length APP ectodomain (*14*)], giving rise to the higher than expected observed BIAcore response. The 1:1 stoichiometry was further confirmed by analytical ultracentrifugation analysis

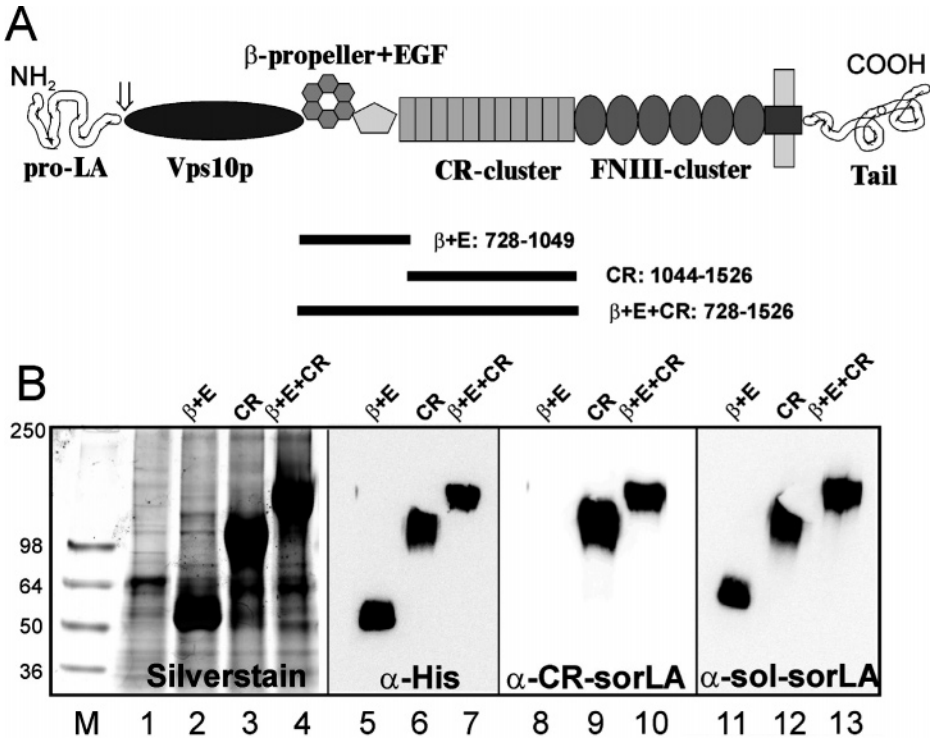

FIGURE 8: Expression of truncated sorLA domains. (A) Depiction of the structural elements of sorLA including (from amino to carboxyl terminus) propeptide (pro-LA, residues 1−53), Vps10p domain (residues 54−727), *β*-propeller, epidermal growth factor repeat (EGF, in combination with the *β*-propeller, equals residues 787−1046), clusters of complement-type repeats (CR, residues 1047−1526) and fibronectin type III domains (FNIII, residues 1527−2107), the transmembrane region (residues 2108−2131), and the cytoplasmatic tail (residues 2132−2186). The amino acid numbering follows that in ref *7*. The arrow (⇓) represents the furin cleavage site for receptor maturation. The extensions of the recombinant sorLA fragments are indicated as horizontal lines below the sorLA polypetide chain. (B) Purified sorLA domains were tested by SDS−PAGE and staining with silver nitrate (lanes 1−4) or immunodetection using antisera directed against the His_6 tag (lanes 5−7), the CR cluster (lanes 8−10), or the entire ectodomain of sorLA (lanes 11−13). Key: lane 1, medium from nontransfected 293 EBNA cells; lanes 5, 8, and 11, *β*-propeller + EGF (*β* + E); lanes 6, 9, and 12, CR cluster (CR); lanes 7, 10, and 13, *β*-propeller + EGF + CR cluster (*β* + E + CR).

of the complex formation, where much lower concentrations of d6A were used, not causing problems of aggregation.

Although the binding of d1 may be of minor physiological importance as compared to d6, identification of two independent sorLA recognition motifs may point to a common structural element required for receptor binding. Thus, highly charged basic surface regions have been described for both d1 (*30*) and d6A (*31*), strongly suggesting that these regions associate with negative charged epitopes in sorLA. The surface exposure of conserved acidic residues within the CR domain scaffold is indeed directly responsible for the binding of positive charged regions within ligands, e.g., RAP (*21*, *39*, *40*), where the number of negatively charged side chains have been suggested to directly relate to the CR cluster ligand binding abilities (*21*). This kind of interaction would be very similar to receptor−ligand interactions that have been described for the association of multiple ligands binding to the CR clusters of members of the LDLR family mainly dependent on reciprocal charged ionic interaction (*41*). The analysis in this study lays the groundwork for further elucidation of the molecular determinants at the atomic level.

Dissection of the APP and sorLA interaction raises several important issues regarding the (patho)physiological roles of the precursor protein. Foremost, these data shed light on the molecular mechanisms that regulate the intracellular fate of APP in neurodegenerative diseases. Because targeting of APP to distinct subcellular compartments determines processing into amyloidogenic products, much attention has focused on cellular factors that interact with APP and regulate its trafficking. Previously, LRP1 and LRP1B (both members of the LDLR superfamily) have been implicated in internalization of APP from the cell surface (*42*, *43*) and shown to interfere with processing in vitro (*29*, *44*). The relevance of sorLA for APP processing and AD progression is supported by the observation that the receptor recognizes d6, which is common to all APP variants as compared to the target site d4 for LRP1, a domain that is not present in the neuronal variant APP_{695} (*45*, *46*). Because interaction of APP with sorLA prevents processing into A*β*, one can envision a scenario where small molecules that foster interaction between d6 and the CR domains may be applied as therapeutic drugs to interfere with amyloid peptide production in patients.

As well as highlighting an important concept in AD progression, sorLA and APP interaction domains may be central to the normal physiological function of APP and related proteins. Although the exact function of the precursor protein in neurons and other cell types is still not resolved, experimental evidence suggests several activities including synaptogenesis, neurite outgrowth (*47*), and cell survival (*48*) in neurons or cell proliferation and motility (*49*) in peripheral tissues. All of these activities may potentially be affected by the presence of sorting receptors determining the intracellular fate of APP. As d6 represents a highly conserved

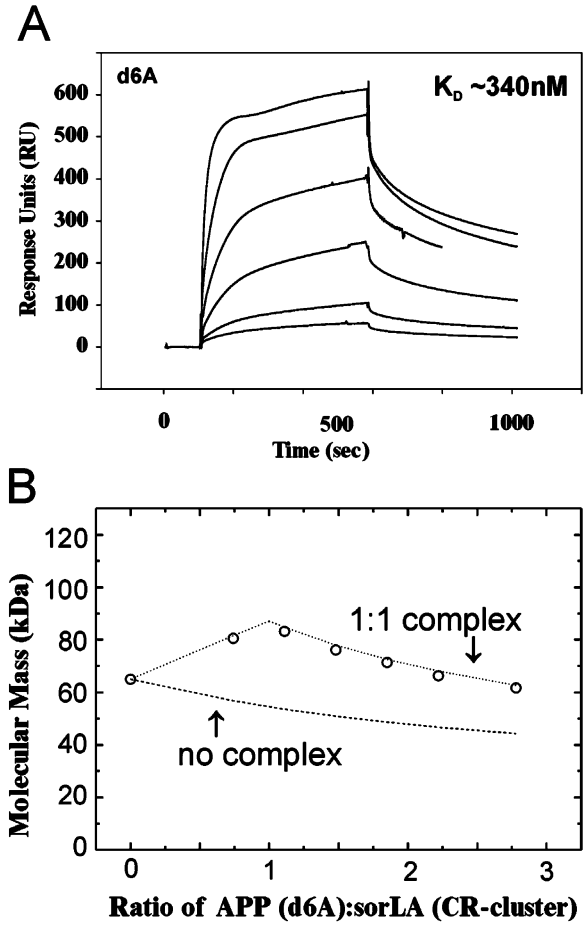

FIGURE 9: Stoichiometric complex formation between APP-d6 and the sorLA CR cluster. (A) Surface plasmon resonance binding analysis of concentration-dependent binding of d6A (0.1, 0.2, 0.5, 1.0, 2.0, and 5.0 μM) to the sorLA CR cluster. Kinetic parameters for the interaction are provided in Table 2B. (B) Molecular mass analysis by ultracentrifugation demonstrates complex formation between APP-d6A and sorLA-CR cluster. The sorLA fragment concentration was kept constant while the concentration of the APP domain was varied to give the indicated input ratios. The maximal M_w is observed for a 1:1 molar ratio of both proteins. Open circles indicate the actual data points. Lines correspond to theoretical weight-average molecular masses for complete (dotted) or absent (dashed) interaction between d6A and the CR cluster.

part of the APP polypeptide chain (*32*), interaction of sorLA with additional members of the APP family, e.g., amyloid precursor-like proteins-1 and -2, by which APP shares overlapping functions (*50*, *51*), also seems plausible. Finally, another interesting aspect of sorLA and APP interaction relates to the identification of cell surface receptors for sAPP. The soluble ectodomain of APP released by α-secretase cleavage has long been suspected to perform distinct physiological functions as a signaling molecule via hitherto unknown cell surface receptor pathways (reviewed in ref *52*). Since d6 is an integral part of the sAPP molecule, the soluble ectodomain is likely to bind to sorLA, as does the full-length precursor, suggesting a possible role for the receptor molecules in sAPP signaling on the cell surface.

ACKNOWLEDGMENT

We are indebted to D. Vetter, J. Zenker, and M. Bundsgaard for technical assistance and to C. M. Petersen (University of Aarhus) for providing anti-sorLA antisera.

SUPPORTING INFORMATION AVAILABLE

One figure showing control sensorgrams for the surface plasmon resonance analysis. This material is available free of charge via the Internet at http://pubs.acs.org.

REFERENCES

1. Motoi, Y., Aizawa, T., Haga, S., Nakamura, S., Namba, Y., and Ikeda, K. (1999) Neuronal localization of a novel mosaic apolipoprotein E receptor, LR11, in rat and human brain, *Brain Res. 833*, 209−215.
2. Hermans-Borgmeyer, I., Hampe, W., Schinke, B., Methner, A., Nykjær, A., Süsens, U., Fenger, U., Herbarth, B., and Schaller, H. C. (1998) Unique expression pattern of a novel mosaic receptor in the developing cerebral cortex, *Mech. Dev. 70*, 65−76.
3. Nykjær, A., Willnow, T. E., and Petersen, C. M. (2005) p75^{NTR}—live or let die, *Curr. Opin. Neurobiol. 15*, 49−57.
4. Willnow, T. E., Nykjær, A., and Herz, J. (1999) Lipoprotein receptors: new roles for ancient proteins, *Nat. Cell Biol. 1*, E157−E162.
5. Nykjær, A., and Willnow, T. E. (2002) The low-density lipoprotein receptor gene family: a cellular Swiss army knife?, *Trends Cell Biol. 12*, 273−280.
6. Jacobsen, L., Madsen, P., Jacobsen, C., Nielsen, M. S., Gliemann, J., and Petersen, C. M. (2001) Activation and functional characterization of the mosaic receptor SorLA/LR11, *J. Biol. Chem. 276*, 22788−22796.
7. Jacobsen, L., Madsen, P., Moestrup, S. K., Lund, A. H., Tommerup, N., Nykjær, A., Sottrup-Jensen, L., Gliemann, J., and Petersen, C. M. (1996) Molecular characterization of a novel human hybrid-type receptor that binds the α_2-macroglobulin receptor-associated protein, *J. Biol. Chem. 271*, 31379−31383.
8. Taira, K., Bujo, H., Hirayama, S., Yamazaki, H., Kanaki, T., Takahashi, K., Ishii, I., Miida, T., Schneider, W. J., and Saito, Y. (2001) LR11, a mosaic LDL receptor family member, mediates the uptake of ApoE-rich lipoproteins in vitro, *Arterioscler. Thromb. Vasc. Biol. 21*, 1501−1506.
9. Gliemann, J., Hermey, G., Nykjær, A., Petersen, C. M., Jacobsen, C., and Andreasen, P. A. (2004) The mosaic receptor sorLA/LR11 binds components of the plasminogen activating system and PDGF-BB similarly to low density lipoprotein receptor-related protein (LRP1) but mediates slow internalization of bound ligand, *Biochem. J. 381*, 203−212.
10. Westergaard, U. B., Sørensen, E. S., Hermey, G., Nielsen, M. S., Nykjær, A., Kirkegaard, K., Jacobsen, C., Gliemann, J., Madsen, P., and Petersen, C. M. (2004) Functional organization of the sortilin Vps10p domain, *J. Biol. Chem. 279*, 50221−50229.
11. Kanaki, T., Bujo, H., Hirayama, S., Ishii, I., Morisaki, N., Schneider, W. J., and Saito, Y. (1999) Expression of LR11, a mosaic LDL receptor family member, is markedly increased in atherosclerotic lesions, *Arterioscler. Thromb. Vasc. Biol. 19*, 2687−2695.
12. Zhu, Y., Bujo, H., Yamazaki, H., Hirayama, S., Kanaki, T., Takahashi, K., Shibasaki, M., Schneider, W. J., and Saito, Y. (2002) Enhanced expression of the LDL receptor family member LR11 increases migration of smooth muscle cells in vitro, *Circulation 105*, 1830−1836.
13. Zhu, Y., Bujo, H., Yamazaki, H., Ohwaki, K., Jiang, M., Hirayama, S., Kanaki, T., Shibasaki, M., Takahashi, K., Schneider, W. J., and Saito, Y. (2004) LR11, an LDL receptor gene family member, is a novel regulator of smooth muscle cell migration, *Circ. Res. 94*, 752−758.
14. Andersen, O. M., Reiche, R., Schmidt, V., Gotthardt, M., Spoelgen, R., Behlke, J., Von Arnim, C. A., Breiderhoff, T., Jansen, P., Wu, X., Bales, K. R., Cappai, R., Masters, C., Gliemann, J., Mufson, E. J., Hyman, B. T., Paul, S. M., Nykjær, A., and Willnow, T. E. (2005) SorLA/LR11, a neuronal sorting receptor that regulates processing of the amyloid precursor protein, *Proc. Natl. Acad. Sci. U.S.A. 102*, 13461−13466.
15. Helmuth, L. (2003) Detangling Alzheimer's disease. New insights into the biological bases of the most common cause of dementia are pointing to better diagnostics and possible therapeutics, *Sci. Aging Knowl. Environ. 2003*, oa2.
16. Mattson, M. P. (2004) Pathways towards and away from Alzheimer's disease, *Nature 430*, 631−639.
17. Selkoe, D. J. (1999) Translating cell biology into therapeutic advances in Alzheimer's disease, *Nature 399*, A23−A31.

18. Selkoe, D. J. (1998) The cell biology of β-amyloid precursor protein and presenilin in Alzheimer's disease, *Trends Cell Biol. 8*, 447−453.
19. De Strooper, B., and Annaert, W. (2000) Proteolytic processing and cell biological functions of the amyloid precursor protein, *J. Cell Sci. 113*, 1857−1870.
20. Scherzer, C. R., Offe, K., Gearing, M., Rees, H. D., Fang, G., Heilman, C. J., Schaller, H. C., Levey, A. I., and Lah, J. J. (2004) ApoE receptor LR11 in Alzheimer's disease: Gene profiling of lymphoblasts mirrors changes in the brain, *Arch. Neurol. 61*, 1200−1205.
21. Andersen, O. M., Christensen, L. L., Christensen, P. A., Sørensen, E. S., Jacobsen, C., Moestrup, S. K., Etzerodt, M., and Thøgersen, H. C. (2000) Identification of the minimal functional unit in the low-density lipoprotein receptor-related protein for binding the receptor-associated protein (RAP), *J. Biol. Chem. 275*, 21017−21024.
22. Andersen, O. M., Benhayon, D., Curran, T., and Willnow, T. E. (2003) Differential binding of ligands to the apolipoprotein E receptor 2, *Biochemistry 42*, 9355−9364.
23. McKinstry, W. J., Feil, S. C., Galatis, D., Cappai, R., and Parker, M. W. (2005) in *Amyloid Precursor Protein. A Practival Approach* (Xu, H., and Xia, W., Eds.) pp 29−40, CRC Press, Boca Raton, FL.
24. Barnham, K. J., McKinstry, W. J., Multhaup, G., Galatis, D., Morton, C. J., Curtain, C. C., Williamson, N. A., White, A. R., Hinds, M. G., Norton, R. S., Beyreuther, K., Masters, C. L., Parker, M. W., and Cappai, R. (2003) Structure of the Alzheimer's disease amyloid precursor protein copper binding domain. A regulator of neuronal copper homeostasis, *J. Biol. Chem. 278*, 17401−17407.
25. Behlke, J., Ristau, O., and Schönfeld, H. J. (1997) Nucleotide-dependent complex formation between the *Escherichia coli* chaperonins GroEL and GroES studied under equilibrium conditions, *Biochemistry 36*, 5149−5156.
26. Berezovska, O., Ramdya, P., Skoch, J., Wolfe, M. S., Bacskai, B. J., and Hyman, B. T. (2003) Amyloid precursor protein associates with a nicastrin-dependent docking site on the presenilin 1-γ-secretase complex in cells demonstrated by fluorescence lifetime imaging, *J. Neurosci. 23*, 4560−4566.
27. Bacskai, B. J., Skoch, J., Hickey, G. A., Allen, R., and Hyman, B. T. (2003) Fluorescence resonance energy transfer determinations using multiphoton fluorescence lifetime imaging microscopy to characterize amyloid-β plaques, *J. Biomed. Opt. 8*, 368−375.
28. Pietrzik, C. U., Busse, T., Merriam, D. E., Weggen, S., and Koo, E. H. (2002) The cytoplasmic domain of the LDL receptor-related protein regulates multiple steps in APP processing, *EMBO J. 21*, 5691−5700.
29. Zerbinatti, C. V., Wozniak, D. F., Cirrito, J., Cam, J. A., Osaka, H., Bales, K. R., Zhuo, M., Paul, S. M., Holtzman, D. M., and Bu, G. (2004) Increased soluble amyloid-β peptide and memory deficits in amyloid model mice overexpressing the low-density lipoprotein receptor-related protein, *Proc. Natl. Acad. Sci. U.S.A. 101*, 1075−1080.
30. Rossjohn, J., Cappai, R., Feil, S. C., Henry, A., McKinstry, W. J., Galatis, D., Hesse, L., Multhaup, G., Beyreuther, K., Masters, C. L., and Parker, M. W. (1999) Crystal structure of the N-terminal, growth factor-like domain of Alzheimer amyloid precursor protein, *Nat. Struct. Biol. 6*, 327−331.
31. Wang, Y., and Ha, Y. (2004) The X-ray structure of an antiparallel dimer of the human amyloid precursor protein E2 domain, *Mol. Cell 15*, 343−353.
32. Dulubova, I., Ho, A., Huryeva, I., Südhof, T. C., and Rizo, J. (2004) Three-dimensional structure of an independently folded extracellular domain of human amyloid-β precursor protein, *Biochemistry 43*, 9583−9588.
33. Willnow, T. E., Rohlmann, A., Horton, J., Otani, H., Braun, J. R., Hammer, R. E., and Herz, J. (1996) RAP, a specialized chaperone, prevents ligand-induced ER retention and degradation of LDL receptor-related endocytic receptors, *EMBO J. 15*, 2632−2639.
34. Hsieh, J. C., Lee, L., Zhang, L., Wefer, S., Brown, K., DeRossi, C., Wines, M. E., Rosenquist, T., and Holdener, B. C. (2003) Mesd encodes an LRP5/6 chaperone essential for specification of mouse embryonic polarity, *Cell 112*, 355−367.
35. Culi, J., and Mann, R. S. (2003) Boca, an endoplasmic reticulum protein required for wingless signaling and trafficking of LDL receptor family members in *Drosophila*, *Cell 112*, 343−354.
36. Culi, J., Springer, T. A., and Mann, R. S. (2004) Boca-dependent maturation of beta-propeller/EGF modules in low-density lipoprotein receptor proteins, *EMBO J. 23*, 1372−1380.
37. Zhang, Y., Wang, Y., Li, X., Zhang, J., Mao, J., Li, Z., Zheng, J., Li, L., Harris, S., and Wu, D. (2004) The LRP5 high-bone-mass G171V mutation disrupts LRP5 interaction with Mesd, *Mol. Cell. Biol. 24*, 4677−4684.
38. Loukinova, E., Ranganathan, S., Kuznetsov, S., Gorlatova, N., Migliorini, M. M., Loukinov, D., Ulery, P. G., Mikhailenko, I., Lawrence, D. A., and Strickland, D. K. (2002) Platelet-derived growth factor (PDGF)-induced tyrosine phosphorylation of the low-density lipoprotein receptor-related protein (LRP). Evidence for integrated co-receptor function between LRP and the PDGF, *J. Biol. Chem. 277*, 15499−15506.
39. Andersen, O. M., Schwarz, F. P., Eisenstein, E., Jacobsen, C., Moestrup, S. K., Etzerodt, M., and Thøgersen, H. C. (2001) Dominant thermodynamic role of the third independent receptor binding site in the receptor-associated protein RAP, *Biochemistry 40*, 15408−15417.
40. Melman, L., Cao, Z.-F., Rennke, S., Paz Marzolo, M., Wardell, M. R., and Bu, G. (2001) High affinity binding of receptor-associated protein to heparin and low-density lipoprotein receptor-related protein requires similar basic amino acid sequence motifs, *J. Biol. Chem. 276*, 29338−29346.
41. Verdaguer, N., Fita, I., Reithmayer, M., Moser, R., and Blaas, D. (2004) X-ray structure of a minor group human rhinovirus bound to a fragment of its cellular receptor protein, *Nat. Struct. Mol. Biol. 11*, 429−434.
42. Cam, J. A., Zerbinatti, C. V., Li, Y., and Bu, G. (2005) Rapid endocytosis of the low-density lipoprotein receptor-related protein modulates cell surface distribution and processing of the β-amyloid precursor protein, *J. Biol. Chem. 280*, 15464−15470.
43. Cam, J. A., Zerbinatti, C. V., Knisely, J. M., Hecimovic, S., Li, Y., and Bu, G. (2004) The LDL receptor-related protein 1B retains β-APP at the cell surface and reduces amyloid-β peptide production, *J. Biol. Chem. 279*, 29639−29646.
44. Kinoshita, A., Whelan, C. M., Smith, C. J., Mikhailenko, I., Rebeck, G. W., Strickland, D. K., and Hyman, B. T. (2001) Demonstration by fluorescence resonance energy transfer of two sites of interaction between the low-density lipoprotein receptor-related protein and the amyloid precursor protein: role of the intracellular adapter protein Fe65, *J. Neurosci. 21*, 8354−8361.
45. Kounnas, M. Z., Moir, R. D., Rebeck, G. W., Bush, A. I., Argraves, W. S., Tanzi, R. E., Hyman, B. T., and Strickland, D. K. (1995) LDL receptor-related protein, a multifunctional ApoE receptor, binds secreted β-amyloid precursor protein and mediates its degradation, *Cell 82*, 331−340.
46. Knauer, M. F., Orlando, R. A., and Glabe, C. G. (1996) Cell surface APP751 forms complexes with protease nexin 2 ligands and is internalized via the low density lipoprotein receptor-related protein (LRP), *Brain Res. 740*, 6−14.
47. Milward, E. A., Papadopoulos, R., Fuller, S. J., Moir, R. D., Small, D., Beyreuther, K., and Masters, C. L. (1992) The amyloid protein precursor of Alzheimer's disease is a mediator of the effects of nerve growth factor on neurite outgrowth, *Neuron 9*, 129−137.
48. Schubert, D., Jin, L.-W., Saitoh, T., and Cole, G. (1989) The regulation of amyloid beta protein precursor secretion and its modulatory role in cell adhesion, *Neuron 3*, 689−694.
49. Schmitz, A., Tikkanen, R., Kirfel, G., and Herzog, V. (2002) The biological role of the Alzheimer amyloid precursor protein in epithelial cells, *Histochem. Cell Biol. 117*, 171−180.
50. Bellingham, S. A., Ciccotosto, G. D., Needham, B. E., Fodero, L. R., White, A. R., Masters, C. L., Cappai, R., and Camakaris, J. (2004) Gene knockout of amyloid precursor protein and amyloid precursor-like protein-2 increases cellular copper levels in primary mouse cortical neurons and embryonic fibroblasts, *J. Neurochem. 91*, 423−428.
51. Herms, J., Anliker, B., Heber, S., Ring, S., Fuhrmann, M., Kretzschmar, H., Sisodia, S., and Muller, U. (2004) Cortical dysplasia resembling human type 2 lissencephaly in mice lacking all three APP family members, *EMBO J. 23*, 4106−4115.
52. Mattson, M. P. (1997) Cellular actions of β-amyloid precursor protein and its soluble and fibrillogenic derivatives, *Physiol. Rev. 77*, 1081−1132.

BI052120V